OPEN ACCESS Freely available online

PLOS ONE

The Internal Organization of Mycobacterial Partition Assembly: Does the DNA Wrap a Protein Core?

Shuo Qian[1], Rebecca Dean[2¤a], Volker S. Urban[1], Barnali N. Chaudhuri[2,3*¤b]

1 Center for Structural Molecular Biology, Biology and Soft Matter Division, Oak Ridge National Laboratory, Oak Ridge, Tennessee, United States of America, **2** Hauptman Woodward Institute, Buffalo, New York, United States of America, **3** Department of Structural Biology, State University of New York, Buffalo, New York, United States of America

Abstract

Before cell division in many bacteria, the ParBs spread on a large segment of DNA encompassing the origin-proximal *parS* site(s) to form the partition assembly that participates in chromosome segregation. Little is known about the structural organization of chromosomal partition assembly. We report solution X-ray and neutron scattering data characterizing the size parameters and internal organization of a nucleoprotein assembly formed by the mycobacterial chromosomal ParB and a 120-meric DNA containing a *parS*-encompassing region from the mycobacterial genome. The cross-sectional radii of gyration and linear mass density describing the rod-like ParB-DNA assembly were determined from solution scattering. A ''DNA outside, protein inside'' mode of partition assembly organization consistent with the neutron scattering hydrogen/deuterium contrast variation data is discussed. In this organization, the high scattering DNA is positioned towards the outer region of the partition assembly. The new results presented here provide a basis for understanding how ParBs organize the *parS*-proximal chromosome, thus setting the stage for further interactions with the DNA condensins, the origin tethering factors and the ParA.

Citation: Qian S, Dean R, Urban VS, Chaudhuri BN (2012) The Internal Organization of Mycobacterial Partition Assembly: Does the DNA Wrap a Protein Core? PLoS ONE 7(12): e52690. doi:10.1371/journal.pone.0052690

Editor: Vladimir N. Uversky, University of South Florida College of Medicine, United States of America

Received October 4, 2012; **Accepted** November 20, 2012; **Published** December 20, 2012

Funding: Funding was provided by The John R. Oishei Foundation. Work at the Stanford Synchrotron Radiation Laboratory was supported by the Department of Energy, Office of Biological and Environmental Research, and by the National Institutes of Health, National Center for Research Resources, Biomedical Technology Program. SANS research at Oak Ridge National Laboratory's Center for Structural Molecular Biology was supported by the Office of Biological and Environmental Research, using ORNL's High Flux Isotope Reactor, sponsored by the Scientific User Facilities Division, Office of Basic Energy Sciences, U.S. Department of Energy. The funders had no role in study design, data collection and analysis, decision to publish, or preparation of the manuscript.

Competing Interests: The authors have declared that no competing interests exist.

* E-mail: barnalichaudhuri1@gmail.com

¤a Current address: Medical Technology Program, The State University of New York at Buffalo, Buffalo, New York, United States of America
¤b Current address: Faculty of Life Sciences and Biotechnology, South Asian University, New Delhi, India

Introduction

An active segregation ensures the equivalent DNA distribution amongst daughter cells, which is a crucial cellular process in bacteria [1–2]. The bacterial partitioning cassette (ParABS) or the segrosome participates in the segregation of many plasmids and chromosomes [1–4]. More than 2/3rd of the sequenced bacterial genomes harbor genes for the segrosome components [5–6]. Based on the nature of the motor protein involved, the segrosomes are classified into three major types [1–2]: type I (involving Walker A Cytoskeletal ATPase or WACA, [7]), type II (involving actin-like ParM ATPase) and type III (involving GTPase). The chromosomal segrosomes exclusively form a subtype of the type I family [1–2], that typically contains a motor protein (ParA, which is a WACA), a centromeric DNA binding protein (ParB) and a set of centromere-like DNA sequence(s) near the origin of replication (*parS*). Chromosomal ParBs spread on the DNA template in the *parS*-adjacent region [8–10] to form the partition assembly, which is a higher-order nucleo-protein complex of unknown nature.

The partition assembly recruits a number of proteins, each with a significant role in the bacterial cell cycle. An interaction between the partition assembly and the ParA is required for the ParABS-mediated DNA movement in many bacteria [3–4], [11–14]. In addition, the partition assembly interacts with the SMC proteins or DNA condensins in *Bacillus subtilis* and *Streptococcus pneumoniae* for accurate chromosome segregation [15–17]. In *Caulobacter crescentus*, the origin-proximal ParB-assembly associates with a polymeric cell-pole organization factor, PopZ, which tethers the origin region to the cell pole [18]. MipZ, which is the essential cell-division site selection protein in *C. crescentus*, interacts with the ParB-DNA assembly at the cell pole while synchronizing the DNA segregation with cell division [19]. The partition assembly directly interacts with the apical growth factor DivIVA in actinobacteria for tethering the chromosomal origin to the cell pole [20]. The precise natures of the interactions between multiple proteins and the partition assembly are not known.

Chromosomal *parS* is typically a conserved, 14 residue long, palindromic 'GTTTCACGTGAAAC' sequence. Sequence analysis identified potential *parS* sites in a number of bacteria [5–6]. A large variability in their numbers, positions and spacing between them has been reported [6]. Recently it has been shown that the *parS* site plays a crucial role in determining the overall genome orientation in *C. crescentus* [21]. The *parS* site appears to nucleate a condensed chromosome conformation, probably due to the assembling of ParBs and DNA condensins [21]. Although much progress have been made on understanding the plasmid-based

partition assemblies of type I and type II categories [22], how the chromosomal ParBs organize the *parS*-encompassing region for segregation is yet to be determined.

The ParABS plays a key role in the mycobacterial cell cycle progression [23–25]. However, little is understood about the organization and function of the ParABS in pathogenic mycobacteria. Previously we described the solution organizations of chromosomal ParB (tbParB) from *Mycobacterium tuberculosis* (MTB) in the apo form [26] and in a complex with the *parS* DNA [27]. Here, we report the internal organization of the partition assembly formed by tbParB and a 120-meric DNA from the MTB genome containing a *parS* site using solution X-ray and neutron scattering (SAXS/SANS) with hydrogen/deuterium (H/D) contrast variation. Our data suggests that the DNA wraps around a protein core in the mycobacterial partition assembly, which serves to organize the DNA in a more compact form. The biological relevance of our result is discussed.

Materials and Methods

Materials

The tbParB was expressed and purified as described previously [27]. All experiments were performed in buffer A (10–50 mM Tris. HCl pH 8, 150 mM NaCl and 10% glycerol), unless otherwise noted. A 120-meric DNA and its complementary DNA (henceforth referred to as D120, CTGCTGCAGCGCCGATGGGGGTGTCGAATTCTGTCGATGTTTCACGTGAAACATTCATCGTCGGATTGTGCGCGGCCTCAGGCGTCGGTGTCGGTGGTGTCATTTCCCGCTGGAATGGTT, the *parS* sequence is underlined) were chemically synthesized, gel purified and annealed by heating at 95 C followed by slow cooling (The Keck oligonucleotide synthesis facility, Yale University). The duplex D120 was incubated with purified tbParB, co-purified as a nucleoprotein complex using a size-exclusion column (Superdex200, GE healthcare, Milwaukee, Wisconsin) and concentrated prior to the scheduled solution scattering experiments.

Small Angle X-ray Scattering (SAXS)

SAXS experiments on the tbParB-D120 complex were performed at the BL4-2 beamline at the Stanford Synchrotron Radiation Laboratory (SSRL, [28–29]), at an X-ray energy of ~11 keV and 2.5 m sample-to-detector distance. Silver behenate was used as a standard calibration to convert detector pixel value to the X-ray scattering vector q in $Å^{-1}$, defined as $q = 4\pi\sin(\theta)/\lambda$, where 2θ is the scattering angle and λ is the wavelength of the incident X-ray beam. All data were collected using the autosampler controlled by Blu-Ice [28]. The subsequent data reduction steps, such as radial integration, intensity scaling, frame-averaging and back-ground subtraction, were performed by the program SASTOOL [29].

Solution Neutron Scattering (SANS) with H/D-contrast Variation

The tbParB-DNA complex at 1.9 mg/ml protein concentration was dialyzed in 10 mM Tris.HCl at pH 8.0, 10% glycerol and different amounts of D_2O (Cambridge Isotope Laboratories, Inc, www.isotope.com) prior to neutron scattering data collection. Neutron scattering data were collected at the CG-3 Bio-SANS instrument [30] at the High Flux Isotope Reactor facility of Oak Ridge National Laboratory (ORNL). A complete set of data covering the momentum transfer range q from 0.007 $Å^{-1}$ to 0.38 $Å^{-1}$ were taken at two sample-to-detector distances 2.5 m and 6.8 m with wavelength $\lambda = 6$ Å and a spread $\Delta\tilde{\lambda}\lambda = 0.15$. Samples were measured in the quartz "banjo" cells (Hellma USA, Plainview, NY) with 1 mm path length and 3–4 hours exposure time. Two dimensional data from the 192 by 192 pixels position-sensitive detector (ORDELA, Inc., Oak Ridge, TN) were corrected for the detector dark current, pixel sensitivity and then azimuthally averaged to produce the one dimensional scattering profile I(q) *versus* q, which was normalized to the incident neutron beam flux. Data reduction was performed by software developed at the neutron scattering facilities of ORNL. After merging the data from two sample-to-detector distances, the backgrounds from the buffer and quartz cell, as well as the incoherent scattering were subtracted from the scattering profiles. Experimental scattering intensity was converted to absolute neutron scattering cross-section per unit volume in units of cm^{-1} by using a calibration standard of known cross-section (Figure S1). The percentages of D_2O in the H/D contrast measurement series (12.0%, 73.5% and 85.5%) were calculated using the neutron transmission data. Data analysis and size calculations were performed using MULCH [31] and the ATSAS suite of software including PRIMUS and GNOM [32–34].

Results

The Size of Partition Assembly in Solution

The solution scattering technique was employed to characterize the size parameters of a complex between the tbParB and a 120-meric DNA containing a 14-meric *parS* site (tbParB-D120, Figure 1a). Unlike many other bacterial plasmids and chromosomes, *Mycobacteria* contains very few *parS* sites [6], [23]. Two 14-meric *parS* sites have been identified in the origin-proximal region of the MTB genome, which are separated by about 850 nucleotides. The 120-meric DNA contains sequences encompassing one *parS* site within the MTB chromosome (see Experimental Procedures section). The tbParB-D120 assembly formation was confirmed by electron microscopy (unpublished data). The average radius of gyration (R_g) over three concentrations and the real-space R_g of the tbParB-D120, determined from the conventional Guinier plots and the pair-distribution function (P(r)), are 94.3 Å ($q.R_g < 1.2$) and 96.5 Å, respectively (Figure 1a, inset). Averaged cross-sectional radius of gyration (R_{xs}) of the tbParB-D120 was determined to be 28.1 Å from the slopes of the modified Guinier plots at three concentrations (Figure 1b) [35]. R_g and R_{XS} values determined at three concentrations were within 5% of the average. The maximum particle diameters from the P(r) and the cross-sectional pair distribution function ($P_{XS}(r)$) were assigned to be 350 Å and 114 Å (Figures 1c and 1d). The diameter D and the length L of a uniform rod-shaped particle were estimated from the radii of gyrations (R_g and R_{XS}), as follows:

$$D = 2R_{xs}\sqrt{2}$$

$$L^2 = 12(R_g^2 - R_{xs}^2)$$

A length-to-diameter ratio larger than 3 is consistent with a rod-like shape of the tbParB-D120 assembly. The shape of modified Guinier plot and a left-skewed profile of the pair distribution function (Figure 1b–c) further supports a rod-like extended structure of the tbParB-D120 in solution.

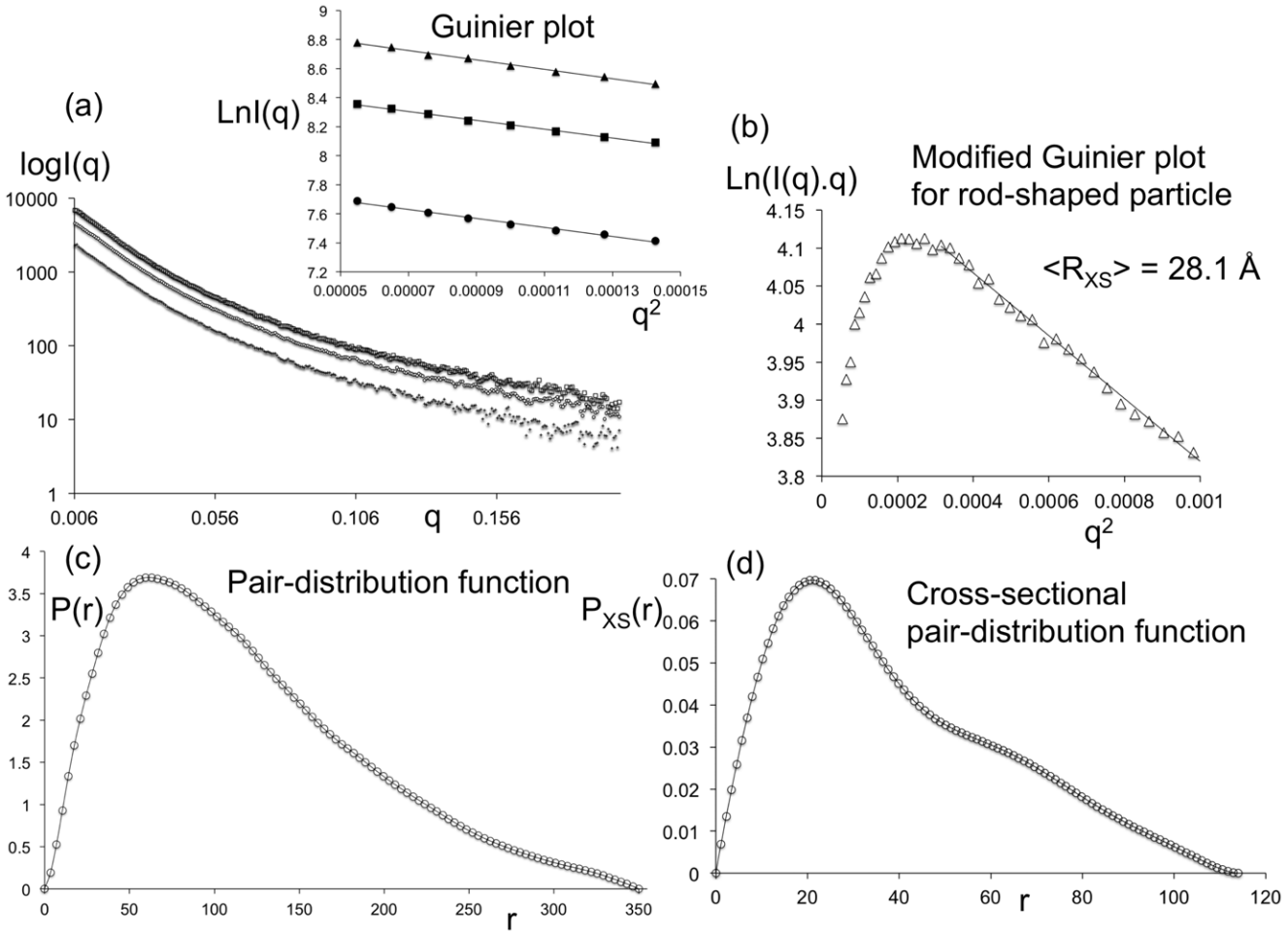

Figure 1. The size of tbParB-D120 assembly derived from the SAXS data. (a) Intensity (I) in arbitrary unit *versus* momentum transfer q in $Å^{-1}$ are plotted at 3 different concentrations. The Guinier plot (lnI(q) *versus* q^2, q in $Å^{-1}$; $lnI(q) = lnI(0) - R_g^2 q^2/3$) is shown in the inset. These and other graphs presented in this work are prepared using Excel® (Microsoft® corporation). A linear trend-line fitted to the data points is shown in each case. (b) The modified Guinier plot for rod-shaped particle (lnI(q)q *versus* q^2, q in $Å^{-1}$, $lnI(q)q = ln(I(q)q)_{q\to 0} - R_{XS}^2 q^2/2$) is shown. (c) The pair-distribution function P(r) *versus* pair-wise distance r in Å. The pair functions shown here and in the figure 5 were calculated with the following boundary conditions: $P(r=0)=0$ and $P(r \geq D_{max})=0$. (d) The cross-sectional pair-distribution function ($P_{XS}(r)$) *versus* pair-wise distance r in Å.
doi:10.1371/journal.pone.0052690.g001

Stuhrmann Plot Suggests a "DNA Outside, Protein Inside" Organization of the Partition Assembly

The neutron scattering contrast variation data can aid in differentiating between two topologically distinct scenarios in a low-resolution sense: (a) the "DNA-inside, protein-outside" model and (b) the "DNA-outside, protein-inside" model (Figure 2a–b). The previous successes of contrast variation in identifying the correct topology for several nucleoprotein assemblies [36–39] prompted us to apply this technique to elucidate the organization of the partition assembly.

To determine the internal topology of the partition assembly, we analyzed the Stuhrmann plot (Figure 3) [40–41];

$$R_g^2 = R_m^2 + \alpha\frac{1}{\Delta\rho} - \beta\frac{1}{\Delta\rho^2}$$

where $\Delta\rho$ is the contrast, R_m is the radius of gyration of the entire particle at infinite contrast and the α and β are two contrast-independent parameters. The above reduces to a linear equation when β equals 0. A positive slope of the Stuhrmann plot ($\alpha > 0$) indicated that on average, the DNA, which has a higher scattering length density than protein, is located towards the peripheral region of the rod (Figure 3). A linear Stuhrmann plot ($\beta = 0$) suggested a two-component system with coincident centers of mass [41], which is consistent with a "DNA outside, protein inside" filament model with two co-axial polymers (Figure 2). Although we have a limited number of data points, the slope of the Stuhrmann plot clearly supports a "DNA outside, protein inside" organization of the partition assembly.

A Reduced Cross-sectional Size Near the DNA Match Point Supports a "DNA Outside, Protein Inside" Model

In order to further ascertain a "DNA outside, protein inside" model, we compared the cross-sectional sizes of the partition assembly derived from the SANS datasets at different % of D_2O. At around ~65–70% D_2O, which is the so-called DNA match-point, the scattering contribution from DNA component of a protein-DNA assembly will effectively disappear or be "matched out" by the solvent. A "DNA-inside" model will behave like a hollow cylinder near the DNA match point (Figure 2a). Contrariwise, the size of a "DNA-outside" model near the

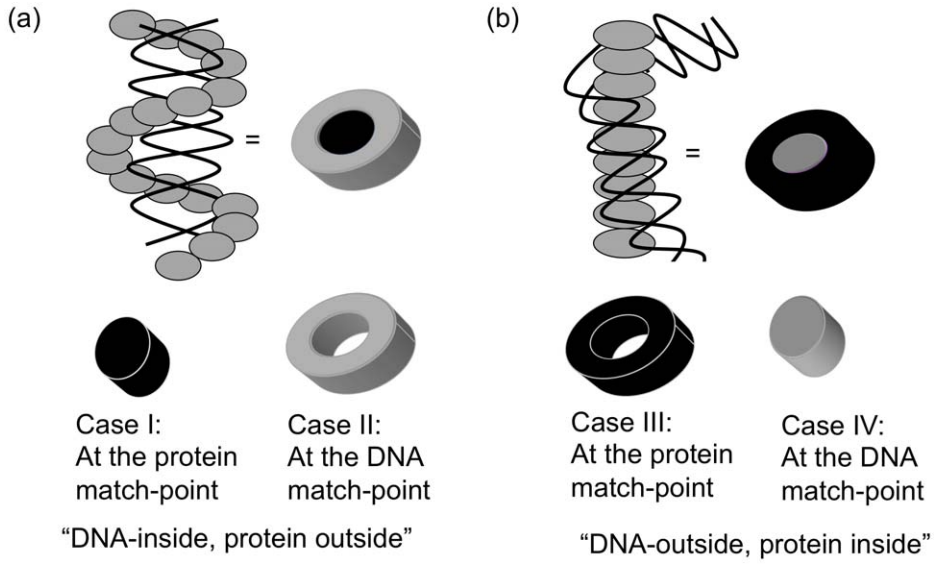

Figure 2. Hypothetical three-dimensional organizations of the partition assembly. Two topologically alternative scenarios can be proposed: (a) a "DNA inside, protein outside" model or (b) a "DNA outside, protein inside" model. The DNA is shown as black line, proteins are shown as grey beads. These models can be described as composite cylinders for low-resolution solution scattering experiments. Anticipated shapes at the protein and the DNA match-point for both models (as narrower or hollow cylinders) are shown as cartoons (case I–IV). The handedness and scale are arbitrary. We note that solution scattering cannot distinguish between the left- and the right-handed senses.
doi:10.1371/journal.pone.0052690.g002

DNA-match point will shrink due to the lack of any scattering contribution from the outer DNA-occupied regions (Figure 2b).

We compared the cross-sectional pair distribution functions ($P_{xs}(r)$, calculated using the option 4 in GNOM, [42–43]) of tbParB-D120 SANS datasets (Figure 4). The cross-sectional maximal diameters obtained from the $P_{xs}(r)$ are 93 Å, 78 Å and 85 Å for the "12.0% D_2O", "73.5% D_2O" and the "85.5% D_2O" datasets respectively. Changes in the shapes of the $P_{xs}(r)$ functions as well as the relative magnitudes of the maximal diameters are consistent with the expected shrinkage of the cross-sectional size near the DNA match-point ("73.5% D_2O") in a "DNA outside" model. A 15 Å change in the maximal cross-sectional size between the 73.5% and the 12.0% dataset suggests that the DNA is loosely wound around a protein core.

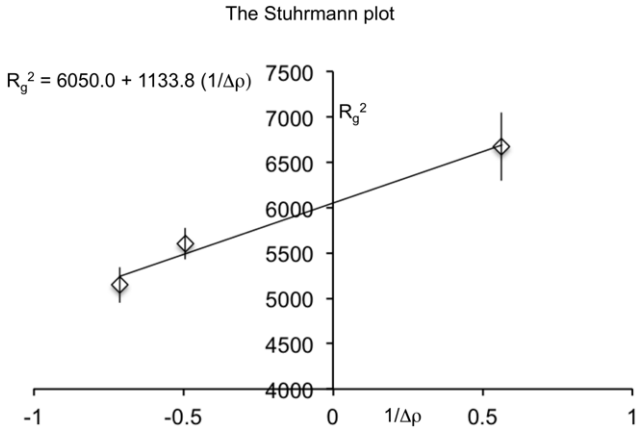

Figure 3. The Stuhrmann plot (R_g^2 *versus* $\Delta\rho^{-1}$, $\Delta\rho$ in 10^{10} cm^{-2}, R_g in Å) obtained from the SANS dataset of the tbParB-D120 assembly. The real space radii of gyration derived from the corresponding pair distribution functions were used for the calculation of Stuhrmann plot. A straight-line fitted to the data ($R^2 = 0.98$) is shown in black.
doi:10.1371/journal.pone.0052690.g003

Linear Mass Density Analysis

Solution scattering data allows an estimation of linear mass density or the mass per unit length of a filament [35], [44]. The intercept (Figure 5) of the modified Guinier plot of the "73.5% D_2O" dataset provided an estimate of the mass per unit length (M/L in Da/Å) of the protein segment of the tbParB-D120 assembly at 1.9 mg/ml protein concentration.

$$\frac{M}{L} = \frac{1000 \cdot I_{XS}(0) \cdot d^2 \cdot N_A}{\pi \cdot C \cdot (\Delta\rho^2)}$$

where $I_{xs}(0)$ is the intercept of the rod-like Guinier plot in cm^{-1}, d is the density (1.35 g/cm^3), N_A is the Avogadro number, C is the concentration in g/l and $\Delta\rho$ is the excess scattering in cm^{-2} units. Mass density of the protein component of the tbParB-D120 particle was estimated to be ~3988 Da/Å at 73.5% D_2O, which roughly corresponds to about a protein dimer *per* 20 Å of axial rise. Earlier, we estimated the largest dimension of a tbParB dimer bound to a 22-meric *parS* DNA to be ~92 Å [27]. The averaged shape of tbParB-*parS* obtained from the *ab initio* shape computations showed that the protein dimer is approximately aligned along the long-axis of DNA [27]. More than 4-fold (20 Å/92 Å) reduction in the projected length of tbParB dimer on the long axis of tbParB-D120 is consistent with protein-induced formation of a DNA super-helix.

Comparison of the mycobacterial chromosomal partition assembly with the other plasmid-based partition assemblies

The homologs and functional analogs of ParB, such as type I SopB and type II ParR, are generally sequentially and/or structurally diverse [22]. However, formation of a higher order

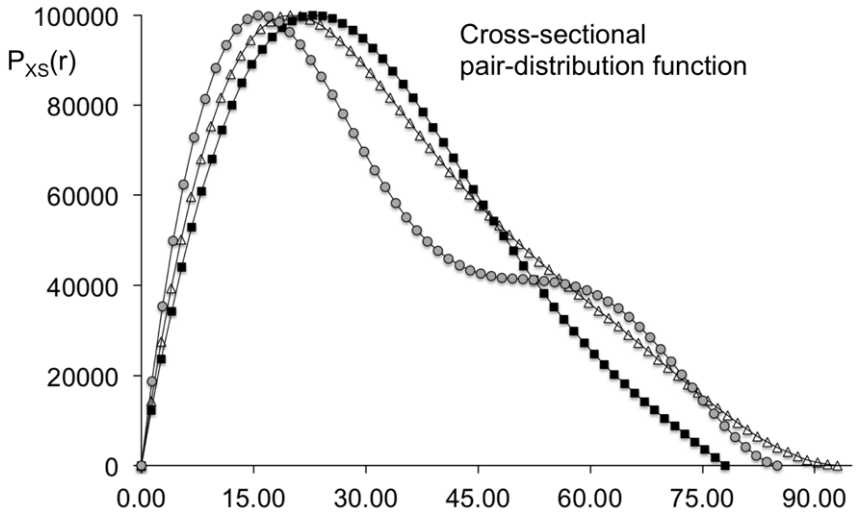

Figure 4. The comparisons of cross-sectional sizes of the tbParB-D120. The cross-sectional pair-distribution functions ($P_{XS}(r)$ *versus* the pair-wise distance r in Å) for the 12.0% (open triangle), 85.5% (grey circle) and 73.5% (black square) D_2O datasets suggests a narrowing of the cross-sectional diameter near the DNA-match point. The $P_{XS}(r)$ functions were scaled to an equal maximal height for visualization purpose.
doi:10.1371/journal.pone.0052690.g004

partition assembly between a centromere binding protein, and the centromere region appears to be a common feature in all cases [22]. The crystal structure of a truncated ParR with the centromeric DNA from the plasmid pSK41 showed a large DNA super-helix formation surrounding a protein interior [45]. Pitch and diameter of this super-helix are ~24 nm and ~18 nm, respectively. The TEM images revealed a ring-like shape of the pB171 ParR-*parC* (equivalent to ParB-*parS*), with a dimension of 15–20 nm [46]. The crystal structure showed a helical array of ParR in the absence of bound DNA, indicating that the observed, ring-like ParR-*parC* could be a two-dimensional projection of helical organization in the TEM micrograph [46]. A similar super-

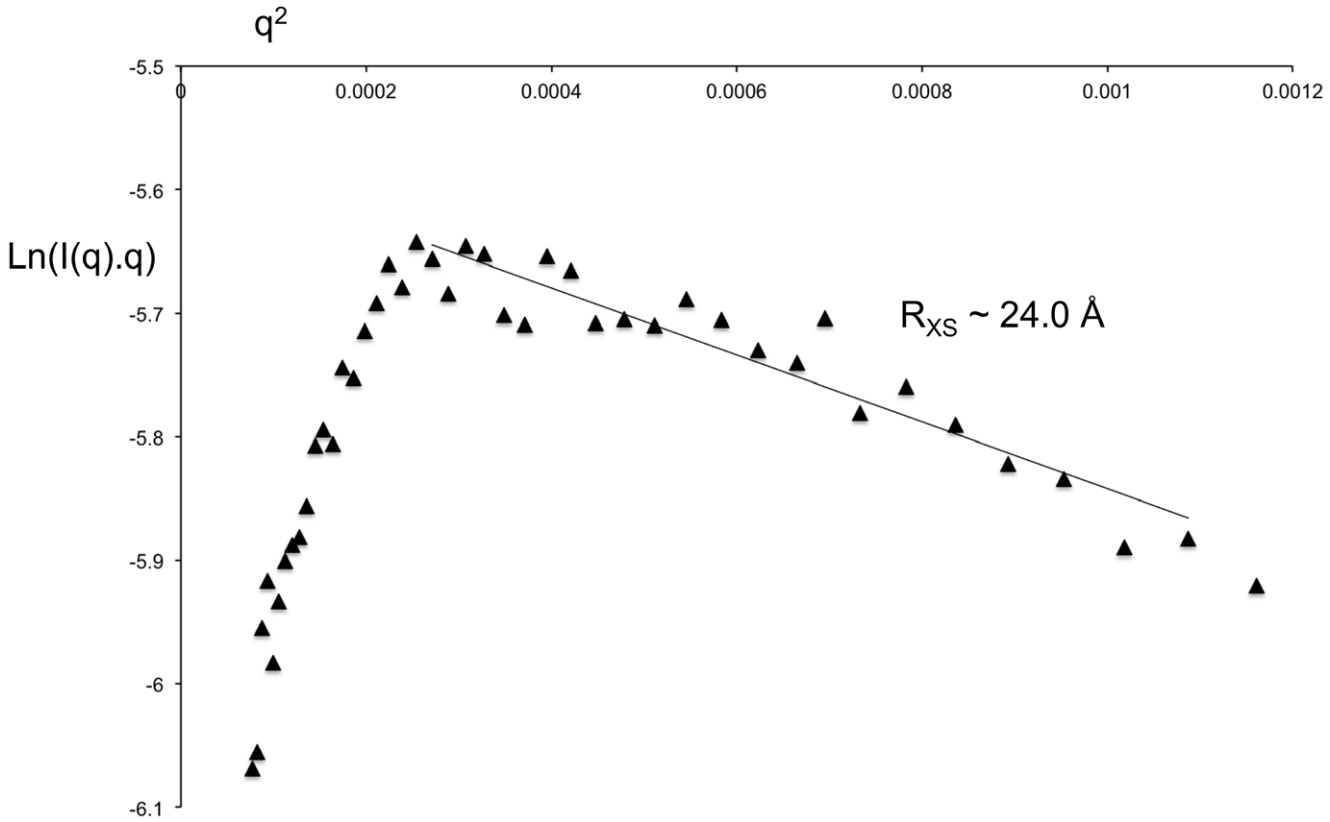

Figure 5. The modified Guinier plot (ln(q.I(q)) *versus* q^2, I in cm^{-1}, q in $Å^{-1}$) of the "73.5% D_2O" dataset. The R_{XS} and mass/length of the protein segment were obtained from the slope and the intercept of this plot.
doi:10.1371/journal.pone.0052690.g005

helical DNA organization was suggested recently for the type III TubR-*tubC* partition assembly [47]. On the other hand, a more extended model of partition assembly that does not involve any DNA wrapping was proposed based on the analyses of SopB-DNA crystal structures [48]. Thus, the internal organization of the mycobacterial partition assembly is similar to some, but not all, of its plasmid-based functional analogs.

Discussion

We report a set of experiment-derived structural parameters describing the mycobacterial partition assembly, such as the cross-sectional radii of gyration and linear mass density. The neutron scattering H/D contrast variation data presented here is consistent with a "DNA outside, protein inside" mode of the partition assembly organization, which is reminiscent of the DNA-histone complex [37–39]. Unlike many previous structural studies on plasmid-based partition assemblies, our data are obtained from a chromosomal partition assembly formed between a DNA with a *parS*-surrounding region and the entire, non-truncated ParB in the solution phase. To the best of our knowledge, this is the first description of the higher order organization of a chromosomal partition assembly, which is a starting point to explore the structural biology of how it recruits different interaction partners, such as ParA, origin tethering factor DivIVA and the SMC proteins, for various biological purposes.

We previously showed that the DNA induces a drastic compaction in the tbParB, which is hypothesized to be required for the higher order partition assembly formation [26]. Our current data suggests a more complex, mutual induced-fit model of the tbParB-DNA interaction. In this model, DNA induces the compaction and polymerization of ParB [26], which in turn induces DNA to form a super-helical array in the outer rim of the protein polymer. Thus, our new data do not support the testable "DNA inside" organization suggested by us earlier [27]. Although our current data do not unambiguously define the geometric parameters of the proposed helical organization, it provides strong evidence that the tbParB organizes a segment of DNA surrounding the *parS* centromere by wrapping it around a protein interior.

Although both plasmid-based SopB and chromosomal ParB belong to the type I group of segrosomes, the organization of the mycobacterial chromosomal partition assembly is intriguingly similar to that of the helical type II ParR-*parC* partition assembly rather than the proposed model of extended SopB-DNA assembly [45–48]. The helical structure of the ParR-DNA assembly seemingly assists in capturing the ParM filament for segregation [45]. While several groups reported nucleotide-induced formations of ParA filaments *in vitro*, the existence of such a ParA filament *in vivo* is still a matter of debate [49–51]. Therefore, whether ParA is captured by utilizing a ParR-*parC*-like mechanism, or by other mechanism, such as by encircling the DNA-coated outer rim of the mycobacterial partition assembly, remains to be determined.

The DNA wrapping by ParB is particularly significant in the light of recent result that the *parS*-proximal region forms a very compact structure extending over ~100kb in *C. crescentus* [21]. This *parS* site was shown to be necessary for the maintenance of global genome orientation within the cell [21]. A role of the DNA condensin, which is known to interact with the partition assembly in many bacteria [15–17], was suggested in the formation of this compact DNA structure of unknown nature [21]. We showed that the chromosomal tbParB, which shares significant sequence similarity with the *Caulobacter* ParB, wraps a *parS*-containing DNA segment *in vitro* in the absence of an additional DNA condensing agent. We suggest that the ParB-induced initial organization prepares the *parS*-encompassing chromosomal segment for the additional large-scale condensation by DNA condensins and the interactions with DivIVA and ParA in the cellular milieu, using yet to be determined mechanisms.

Supporting Information

Figure S1
(TIF)

Acknowledgments

BNC wishes to acknowledge Dr. T. Matsui from SSRL for advice and assistance during the SAXS experiments.

Author Contributions

Conceived and designed the experiments: BNC. Performed the experiments: BNC RD VU. Analyzed the data: BNC VU SQ. Contributed reagents/materials/analysis tools: VU SQ. Wrote the paper: BNC VU SQ.

References

1. Hayes F, Barillà D (2006) The bacterial segrosome: a dynamic nucleoprotein machine for DNA trafficking and segregation. Nature Rev Microbiol 4: 133–43.
2. Gerdes K, Howard M, Szardenings F (2010) Pushing and pulling in prokaryotic DNA segregation. Cell 141: 927–42.
3. Fogel MA, Waldor MK (2006) A dynamic, mitotic-like mechanism for bacterial chromosome segregation. Genes Dev. 20: 3269–3282.
4. Ptacin JL, Lee SF, Garner EC, Toro E, Eckart M, et al. (2010) A spindle-like apparatus guides bacterial chromosome segregation. Nature Cell Biol. 12: 791–8.
5. Gerdes K, Møller-Jensen J, Bugge-Jensen R (2000) Plasmid and chromosome partitioning: surprises from phylogeny. Mol Microbiol. 37: 455–66.
6. Livny J, Yamaichi Y, Waldor MK (2007) Distribution of centromere-like *parS* sites in bacteria: insights from comparative genomics. J Bacteriol. 189: 8693–703.
7. Ingerson-Mahar M, Gitai Z (2012) A growing family: the expanding universe of the bacterial cytoskeleton. FEMS Microbiol Rev. 36: 256–67.
8. Murray H, Ferreira H, Errington J (2006) The bacterial chromosome segregation protein Spo0J spreads along DNA from *parS* nucleation sites. Mol Microbiol. 61: 1352–61.
9. Breier AM, Grossman AD (2007) Whole-genome analysis of the chromosome partitioning and sporulation protein Spo0J (ParB) reveals spreading and origin-distal sites on the *Bacillus subtilis* chromosome. Mol Microbiol. 64: 703–18.
10. Kusiak M, Gapczynska A, Plochocka D, Thomas CM, Jagura-Burdzy G (2011) ParB binding and spreading on DNA determine its biological function in *Pseudomonas aeruginosa*. J Bacteriol. 193: 3342–55.
11. Shebelut CW, Guberman JM, van Teeffelen S, Yakhnina AA, Gitai Z (2010) Caulobacter chromosome segregation is an ordered multistep process. P Natl Acad Sci USA 107: 14194–14198.
12. Vecchiarelli AG, Han YW, Tan X, Mizuuchi M, Ghirlando R, et al. (2010) ATP control of dynamic P1 ParA-DNA interactions: a key role for the nucleoid in plasmid partition. Mol Microbiol. 78: 78–91.
13. Banigan EJ, Gelbart MA, Gitai Z, Wingreen NS, Liu AJ (2011) Filament depolymerization can explain chromosome pulling during bacterial mitosis. PLoS Comput Biol. 7: e1002145.
14. Schofield WB, Lim HC, Jacobs-Wagner C (2010) Cell cycle coordination and regulation of bacterial chromosome segregation dynamics by polarly localized proteins. EMBO J. 29: 3068–81.
15. Sullivan NL, Marquis KA, Rudner DZ (2009) Recruitment of SMC by ParB-parS organizes the origin region and promotes efficient chromosome segregation. Cell 137: 697–707.
16. Gruber S, Errington J (2009) Recruitment of condensin to replication origin regions by ParB/SpoOJ promotes chromosome segregation in *B. subtilis*. Cell 137: 685–96.
17. Minnen A, Attaiech L, Thon M, Gruber S, Veening JW (2011) SMC is recruited to oriC by ParB and promotes chromosome segregation in *Streptococcus pneumoniae*. Mol Microbiol. 81: 676–88.
18. Bowman GR, Comolli LR, Zhu J, Eckart M, Koenig M, et al. (2008) A polymeric protein anchors the chromosomal origin/ParB complex at a bacterial cell pole. Cell 134: 945–55.
19. Thanbichler M, Shapiro L (2006) MipZ, a spatial regulator coordinating chromosome segregation with cell division in Caulobacter. Cell 126: 147–62.

20. Donovan C, Sieger B, Krämer R, Bramkamp M (2012) A synthetic *Escherichia coli* system identifies a conserved origin tethering factor in Actinobacteria. Mol Microbiol. 84: 105–16.
21. Umbarger MA, Toro E, Wright MA, Porreca GJ, Baù D, et al. (2011) The three-dimensional architecture of a bacterial genome and its alteration by genetic perturbation. Mol Cell. 44: 252–64.
22. Schumacher MA (2008) Structural biology of plasmid partition: uncovering the molecular mechanisms of DNA segregation. Biochem J. 412: 1–18.
23. Jakimowicz D, Brzostek A, Rumijowska-Galewicz A, Zydek P, Dołzbłasz A, et al. (2007) Characterization of the mycobacterial chromosome segregation protein ParB and identification of its target in *Mycobacterium smegmatis*. Microbiology. 153: 4050–60.
24. Maloney E, Madiraju M, Rajagopalan M (2009) Overproduction and localization of *Mycobacterium tuberculosis* ParA and ParB proteins. Tuberculosis 89: S65–9.
25. Nisa S, Blokpoel MC, Robertson BD, Tyndall JD, Lun S, et al. (2010). Targeting the chromosome partitioning protein ParA in tuberculosis drug discovery. J Antimicrob Chemother. 65: 2347–58.
26. Chaudhuri BN, Dean R (2011) The Evidence of Large-Scale DNA-Induced Compaction in the Mycobacterial Chromosomal ParB. J Mol Biol. 413: 901–7.
27. Chaudhuri BN, Gupta S, Urban VS, Chance MR, D'Mello R, et al. (2011) A combined global and local approach to elucidate spatial organization of the Mycobacterial ParB-*parS* partition assembly. Biochemistry. 50: 1799–807.
28. Tsuruta H, Brennan S, Rek ZU, Irving TC, Tompkins WH, et al. (1998) A wide-bandpass multilayer monochromator for biological small-angle scattering and fiber diffraction studies. J. Appl. Cryst. 31: 672–682.
29. Smolsky IL, Liu P, Niebuhr M, Ito K, Weiss TM, et al. (2007) Biological small-angle X-ray scattering facility at the Stanford Synchrotron Radiation Laboratory. J. Appl. Cryst. 40 (Supplement): s453–s458.
30. Lynn GW, Heller W, Urban V, Wignall GD, Weiss K, et al. (2006) Bio-SANS - A dedicated facility for neutron structural biology at Oak Ridge National Laboratory. Physica B: Condensed Matter 880: 385–386.
31. Whitten AE, Cai S, Trewhella J (2008) MULCh: modules for the analysis of small-angle neutron contrast variation data from biomolecular assemblies. J Appl Cryst. 41: 222–226.
32. Konarev PV, Petoukhov MV, Volkov VV, Svergun DI (2006) ATSAS 2.1, a program package for small-angle scattering data analysis. J Appl Cryst. 39: 277–286.
33. Konarev PV, Volkov VV, Sokolova AV, Koch MHJ, Svergun DI (2003) PRIMUS - a Windows-PC based system for small-angle scattering data analysis. J Appl Cryst. 36: 1277–1282.
34. Svergun DI (1992) Determination of the regularization parameter in indirect-transform methods using perceptual criteria. J. Appl. Crystallogr. 25: 495–503.
35. Thiyagarajan P, Burkoth TS, Urban V, Seifert S, Benzinger TLS, et al. (2000) pH dependent self assembly of β-amyloid (10–35) and β-amyloid(10–35)-PEG3000. J. Appl. Cryst. 33: 535–539.
36. DiCapua E, Schnarr M, Timmins PA (1989) The location of DNA in complexes of recA protein with double-stranded DNA. A neutron scattering study. Biochemistry 28: 3287–92.
37. Graziano V, Gerchman SE, Schneider DK, Ramakrishnan V (1994) Histone H1 is located in the interior of the chromatin 30-nm filament. Nature. 368: 351–4.
38. Inoko Y, Yamamoto M, Fujiwara S, Ueki T (1992) X-ray scattering study of the shape of the DNA region in nucleosome core particle with synchrotron radiation. J Biochem. 111: 3106.
39. Hjelm RP, Kneale GG, Sauau P, Baldwin JP, Bradbury EM, et al. (1977) Small angle neutron scattering studies of chromatin subunits in solution. Cell 10: 139–51.
40. Ibel K, Stuhrmann HB (1975) Comparison of neutron and X-ray scattering of dilute myoglobin solutions. J. Mol. Biol. 93: 255–265.
41. Perkins SJ (1988) Structural studies of proteins by high-flux X-ray and neutron solution scattering. Biochem J. 254: 313–27.
42. Glatter O (1980) Evaluation of small-angle scattering data from lamellar and cylindrical particles by the indirect transformation method. J Appl Crystallogr. 13: 577–584.
43. Whitten AE, Jeffries CM, Harris SP, Trewhella J (2008) Cardiac myosin-binding protein C decorates F-actin: implications for cardiac function. Proc Natl Acad Sci U S A. 105: 18360–5.
44. Gerchman SE, Ramakrishnan V (1987) Chromatin higher-order structure studied by neutron scattering and scanning transmission electron microscopy. Proc Natl Acad Sci U S A. 84: 7802–6.
45. Schumacher MA, Glover TC, Brzoska AJ, Jensen SO, Dunham TD, et al. (2007) Segrosome structure revealed by a complex of ParR with centromere DNA. Nature. 450: 1268–71.
46. Møller-Jensen J, Ringgaard S, Mercogliano CP, Gerdes K, Löwe J (2007) Structural analysis of the ParR/parC plasmid partition complex. EMBO J. 26: 4413–22.
47. Aylett CH, Löwe J (2012) Superstructure of the centromeric complex of TubZRC plasmid partitioning systems. Proc Natl Acad Sci U S A. 109(41): 16522–7.
48. Schumacher MA, Piro PM, Xu W (2010) Insight into F plasmid DNA segregation revealed by structures of SopB and SopB-DNA complexes. Nucleic Acids Res. 38: 4514–26.
49. Szardenings F, Guymer D, Gerdes K (2011) ParA ATPases can move and position DNA and subcellular structures. Curr Opin Microbiol. 14(6): 712–8.
50. Lutkenhaus J (2012) The ParA/MinD family puts things in their place. Trends Microbiol. 20(9): 411–8.
51. Vecchiarelli AG, Mizuuchi K, Funnell BE (2012) Surfing biological surfaces: exploiting the nucleoid for partition and transport in bacteria. Mol Microbiol. 86(3): 513–23.